Final Report for USGS G20AP00101, 7/1/20 - 6/30/21

"Earthquake Simulators and Next Generation Hazard Models (UCERF4): Collaborative Research with Columbia University and USGS Golden"

Bruce E. Shaw, Columbia University

Lamont Doherty Earth Observatory, Palisades NY 10964, 845-359-2900, FAX: 845-365-8150, shaw@ldeo.columbia.edu

Abstract

With support from this USGS grant, progress on a number of fronts related to earthquake simulators and next generation hazard models has been made. Key progress has been made in three areas. One involves developing and evaluating the simulators in a subduction environment, including coupling a subduction interface fault with upper plate faults. Evaluations of the resulting emergent events include seismicity rates and spatial and clustering effects, and scaling relations for different focal mechanism. A second area of progress involves using the source motions of the simulators under improvements in the source physics the PI developed to generate ground motions and non-ergodic PSHA. A third area of progress is in using simulator events as a guide in helping improve rupture plausibility filters to better estimate fault connectivity and rupture sets for use in UCERF4. Out of this work, one paper has been published, one paper has been submitted for publication, and one additional paper has been submitted in preprint form for review at the USGS. The first one, (*Milner et al.*, 2021), was published in the Bulletin of the Seismological Society of America. The second one, (*Shaw, et al., 2021*) was submitted for publication in the same journal. The third one (*Milner, Shaw, and Field, 2021*) was circulated for review at the USGS. We briefly discuss these three areas below.

Published paper on hazard from fully deterministic physical models

" Toward Physics-Based Nonergodic PSHA: A Prototype Fully-Deterministic Seismic Hazard Model For Southern California" (*Milner, Shaw, et al., 2021*)

We present a nonergodic framework for Probabilistic Seismic Hazard Analysis (PSHA) that is constructed entirely of deterministic, physical models. The use of deterministic ground motion simulations in PSHA calculations is not new (e.g., CyberShake), but prior studies relied on kinematic rupture generators to extend empirical earthquake rupture forecasts. Fully-dynamic models, which simulate rupture nucleation and propagation of static and dynamic stresses, are still computationally intractable for the large simulation domains and many seismic cycles required to perform PSHA. Instead, we employ the Rate-State Earthquake Simulator (RSQSim) to efficiently simulate hundreds of thousands of years of $M > 6.5$ earthquake sequences on the California fault system. RSQSim produces full slip-time histories for each rupture, which, unlike kinematic models, emerge from frictional properties, fault geometry, and stress transfer; all intrinsic variability is deterministic. We use these slip-time histories directly as input to a three-dimensional wave propagation code within the CyberShake platforms to obtain simulated 0.5 Hz ground motions. The resulting three-second spectral acceleration ground motions closely match empirical ground motion model (GMM) estimates of median and variability of shaking well. When computed over a range of sources and sites, the variability is similar to that of ergodic GMMs. Variability

is reduced for individual pairs of sources and sites, which repeatedly sample a single path, which is expected for a nonergodic model. This results in increased exceedance probabilities for certain characteristic ground motions for a source-site pair, while decreasing probabilities at the extreme tails of the ergodic GMM predictions. We present these comparisons and preliminary fully deterministic physics-based RSQSim-CyberShake hazard curves, as well as a new technique for estimating within- and between-event variability through simulation.

We investigate the efficacy of a multi-cycle deterministic earthquake simulator as an extended earthquake rupture forecast (ERF) for use in generating simulated ground motions for probabilistic seismic hazard analyses (PSHA). Although use of deterministic ground motion simulations in PSHA calculations is not new (e.g., CyberShake), prior studies relied on kinematic rupture generators to extend empirical ERFs. Fully-dynamic models, which simulate rupture nucleation and propagation of static and dynamic stresses, are still computationally intractable for the large simulation domains and many seismic cycles required to perform PSHA. Instead, we employ the Rate-State Earthquake Simulator (RSQSim) to efficiently simulate hundreds of thousands of years of M ¿ 6.5 earthquake sequences on the California fault system. RSQSim produces full slip-time histories for each rupture, which, unlike kinematic models, emerge from frictional properties, fault geometry, and stress transfer; all intrinsic variability is deterministic. We use these slip-time histories directly as input to wave propagation codes with the Southern California Earthquake Center (SCEC) BroadBand Platform for one-dimensional models of the Earth and SCEC CyberShake for three-dimensional models to obtain simulated deterministic ground motions.

Some figures illustrating some of the results are included below. Figure 1 illustrates a series of improvements made in the source physics of the simulator to improve the propagation velocity to obtain more realistic directivity effects. These improvements, include: (1) Improving the accuracy of the stiffness matrix by considering not just the finite area of the source patch, but the finite area of the receiver patch as well. (2) Eliminating fixed sliding speed approximation during fast earthquake slip, and replacing it with slip velocity which is determined by the shear impedance relationship. (3) Rather than instantaneous stressing rate updating, introducing a time delay to stress rate updating on other elements which is motivated by a retarded green's function effect from finite wave speeds. An approximation of this effect uses a fixed delay for all elements related to the source patch dimension, to maintain a minimum of updating steps and preserve the fast algorithm. Together these source physics improvements lead to improved propagation velocity.

Figure 2 shows spectra plots of an individual event, and an ensemble of events, compared with empirical Ground Motion Models (GMMs). This gives an example of how the model ground motions are calibrated and validated against empirical observations.

Figure 3 shows an example of a full hazard curve calculated at a single site from the full simulator catalog using a full 3D velocity model in Cybershake. This illustrates a fully deterministic calculation of PSHA using the deterministic sequence of events and source motions from the simulator, with no stochastic aspects.

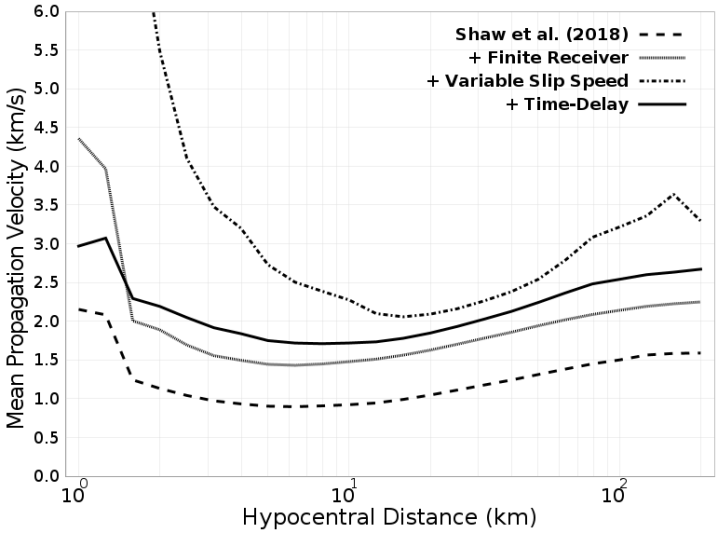

Figure 1: Propagation velocity as a function of patch hypocentral distance for four different RSQSim parameterizations, each of which incorporates a new feature over the previous model. The base model is the catalog used in *Shaw et al.* (2018), plotted with a dashed line. The first modification, plotted with a dotted line, adds a new finite receiver patch capability to the stiffness matrix calculations. The second modification, plotted with a dotted and dashed line, adds variable slip speed capabilities to RSQSim with stepwise updating of sliding velocity on a patch during earthquake slip. The final model, plotted with a solid line and used for PSHA calculations in this study, also includes a time-delay to the static-elastic interaction. From [Milner, Shaw, et al., 2020].

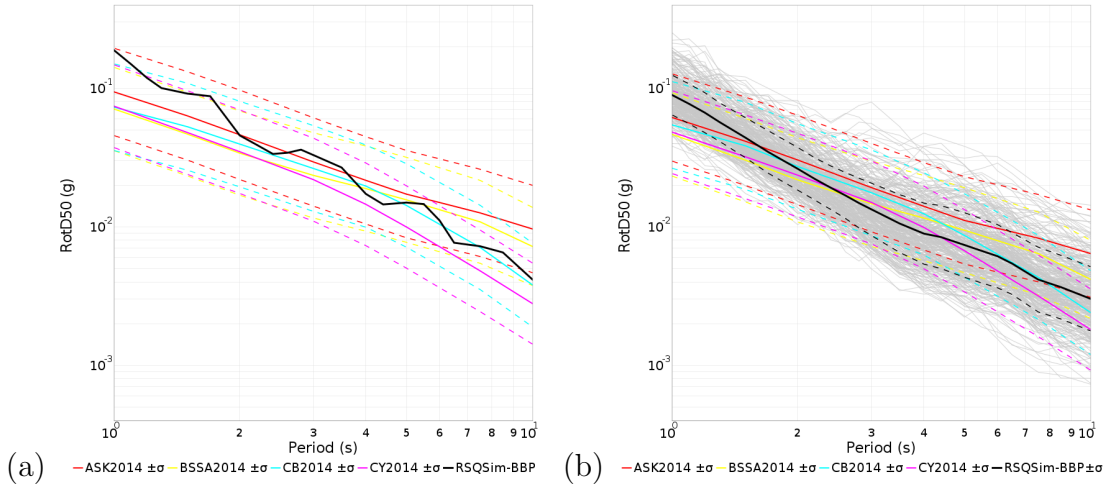

Figure 2: Example ground motions from simulator events compared with Ground Motion Models (GMM). RotD50 spectra for site USC from ruptures on the Mojave section of the San Andreas Fault, computed with a one-dimensional (1D) velocity structure with VS30=500 m/s in the Southern California Earthquake Center (SCEC) BroadBand Platform (BBP). (a) Spectrum for a M 7.48 rupture on the Mojave section of the San Andreas Fault plotted as a thick black line. (b) Spectra for 185 different $7.0 \leq M \leq 7.5$ RSQSim ruptures on the Mojave section of the San Andreas Fault simulated at USC plotted with thin gray lines, the mean of all 185 ruptures as a thick black line, and the mean plus and minus one standard deviation with dashed black lines. GMM comparisons (with plus and minus one standard deviation bounds marked with dashed lines) are plotted with colored lines. GMM predictions are slightly different for (b) because distributions are averaged across those predicted for each of the 185 RSQSim ruptures (rather than for a single M 7.48 rupture in (a)). From [Milner, Shaw, et al., 2020].

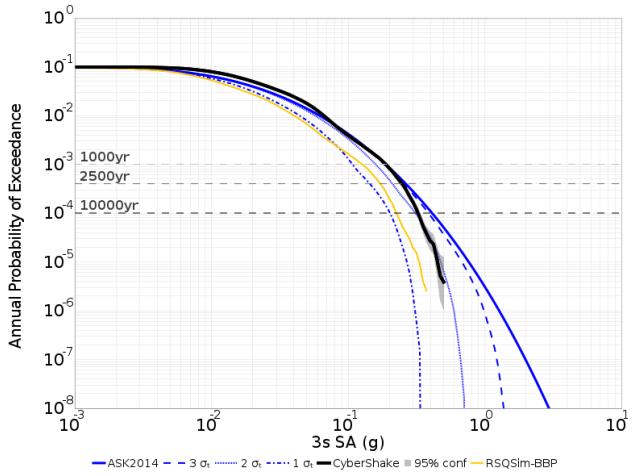

Figure 3: Example of full deterministic PSHA calculation using 3D cybershake and simulator ruptures, done at a single site. RSQSim simulation hazard curves at USC. CyberShake (3D) is plotted with thick, black lines. (a) ASK2014 GMM comparisons curves in blue, with the complete hazard curve plotted as a thick solid line. GMM curves computed from truncated log-normal distributions at three-, two-, and one-sigma are plotted with dashed, dotted, and dotted and dashed lines respectively. The 1D BBP hazard curve is included in yellow, and 95% confidence bounds assuming a binomial distribution (representing sampling uncertainty from a finite catalog duration) on the 3D simulated curve as a gray shaded region. From [Milner, Shaw, et al., 2021].

Submitted paper on subduction zone fault systems

"An Earthquake Simulator for New Zealand" (*Shaw, et al., 2021*)

We present an earthquake simulator for New Zealand. It uses the RSQSim simulator engine based on approximations of the rate-and-state friction equations. The full set of faults considered in the most recent NZ national seismic hazard map are included in the simulator. New simulator methods are introduced that allow for the inclusion and interaction between upper plate faults and a subduction interface fault below them. The simulator generates sequences of complex slip events and a catalog of finite ruptures hundreds of thousands of years in length. Results from the simulator are evaluated through statistical testing and comparison with geological and geophysical observations. These evaluations include a spatial comparison against historical earthquakes, a comparison against rates of events in the instrumental catalog, and a comparison against scaling relations. Consistency of the model with these measures is generally found, though some differences with productivity is noted, due to incomplete modeling of subducting slab features like geodetically inferred spatially dependent creep, and dense faulting in Bay of Plenty faults. Significant emergent aspects of the resulting synthetic catalogue are discussed. These include substantial variability over instrumental catalog timescales, clustering of large events in space and time, and spontaneous ruptures which break both the upper crustal faults and subduction interface co-seismically. An online repository provides the model output and python code for reproducing the figures in the paper and tools for further model output analysis.

Figure 4 shows a map view of the 3D model fault system derived from previous NSHM finite fault source inputs.

Figure 5 compares two model catalogs with the historical New Zealand catalog. Figure 5a shows a 5000 year model catalog, giving a picture of the long-term seismicity. Figure 5b shows a 500 year model catalog, showing a catalog similar to, but somewhat longer than, the timescale of the historical catalog (i.e. ∼180 years). Figure 5b illustrates the non-stationary nature of the large events on even these multiple century timescales. It does, however, provide a rough spatial consistency with the historical catalog.

Figure 6 shows average slip versus area, and magnitude versus area on log scale plots. In Figure 6 we see slip scaling approximately as the square root of area, indicated by the black line. Deviations from this occur at small scales, where finite discretization effects occur, leading to saturation of slip above expected values, and for very large aspect ratio events, where slip saturates due to finite seismogenic width corrections [e.g. (*Shaw*, 2009)]. Different focal mechanisms are color coded in the model, and plotted on top of one another, with thrust being red, strike-slip being blue, and normal being green. The finite width saturation is seen in the model for the largest strike-slip (blue colored) events which have the largest length/width aspect ratios, with slip flattening at the largest events. In Figure 6a we also see a feature seen in real seismicity, that the largest events are thrust, the next largest are strike-slip, followed finally by normal faulting events. Color coding in the plot is by the mechanism of the hypocenter. Some events initiating as strike-slip events, and then propagating onto the subduction interface faults and growing to be very large subduction events, can be seen in the scattered occasional blue points ($A > 10^4 km$) in the plot. Events that co-seismically rupture upper plate faults and the subduction interface are of particular potential interest to seismic hazard, and provide opportunities for further study with the simulator.

Figure 6b shows magnitude-area scaling, here not distinguishing between different focal mechanisms. We also see the features observed in slip-area scaling continuing here. For all but the largest aspect ratios, earthquakes generally scale consistent with magnitude scaling approximately as $\log_{10}$ area, indicated by the black line. which shows a generic scaling

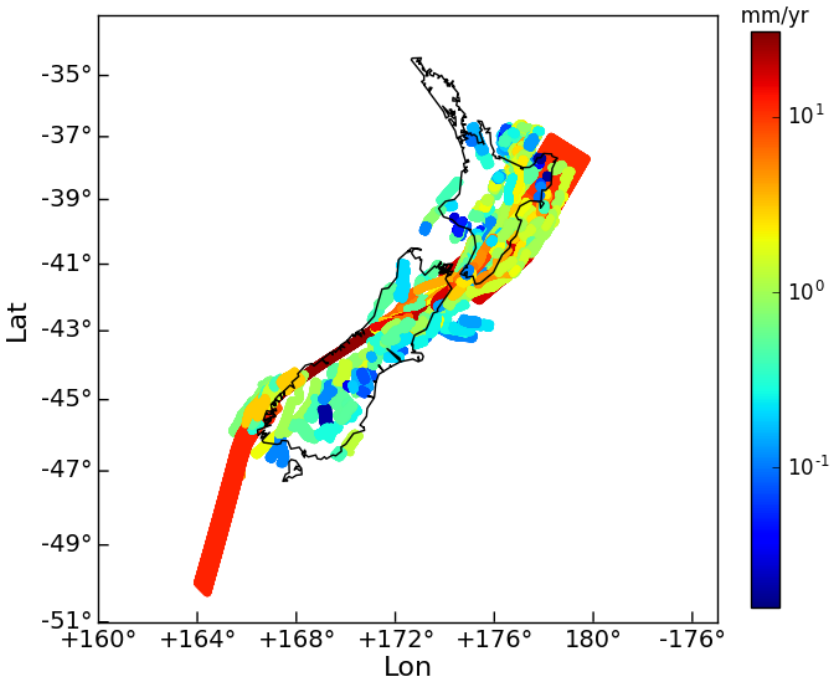

Figure 4: Geological fault model. Colors show slip rate on a logarithmic scale in mm/yr. Fault traces, dip, dip direction, slip rates, and rakes go into constructing this 3D representation. These are the target slip rates that the hybrid loading will then modify to have less singular loading conditions. The fastest moving faults, the Hikurangi subduction on the North Island, the Alpine and Hope faults on the South Island, and the Puysegur-Resolution Ridge subduction to strike-slip below the South Island are highlighted by the warmest colors. From (*Shaw et al.*, 2021)

M= $log_{10}A + C$ with here $C = 4.1$ as a reference value. For small magnitude events, discretization effects lead to more slip and deviations from this. Otherwise consistency with this scaling is seen, to leading order.

Figure 7 shows an example of a large **M**8.3 subduction event on the Southern Hikurangi, which also activates a number of upper plate faults. The event initiated on the subduction interface before rupturing both the subduction interface and a number of upper plate faults in the same event. Listed in order by area participating in the rupture, the upper plate faults activated in this event include the Wellington, Wairarapa, and BooBoo faults. While each event in the model is unique, the co-seismic rupture of this combination of prominent faults was seen to occur a number of times in the catalog, so this is not a rare occurrence during large Southern Hikurangi ruptures in the model. An event of this type, something emergent in the model, presents a striking scenario to contemplate, which contains features reminiscent of the Wairarapa 1855 earthquake.

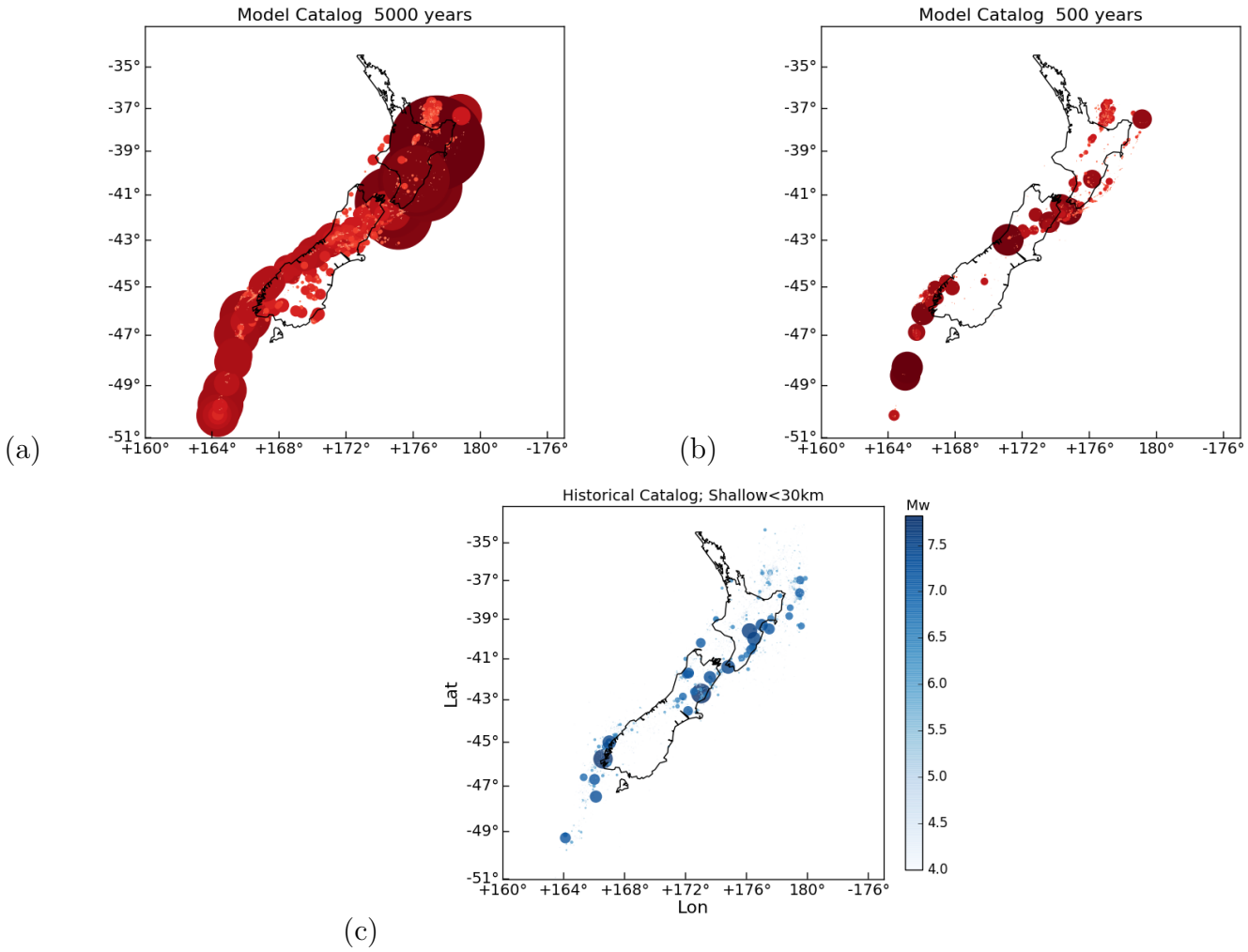

Figure 5: Epicenter map. Color coded by magnitude. Size scaled with rupture area. Plotted sequentially in time, earlier smaller events may be hidden by later larger events. (a) Catalog length here is 5000 years. This is akin to long-term catalog. (b) Catalog length 500 years. (c) Historical and instrumental catalog through 2020 of New Zealand earthquakes, compiled by GeoNet. Blue colormap highlights observed earthquakes. Area of catalog events proportional to $10^{\mathbf{M}}$ for magnitude $\mathbf{M}$. Only shallow (above $30km$ depth) events are plotted, since the model aims only to simulate shallow events. To first order we see spatial consistency. Some spatial differences in medium and large event productivity are seen in Central and Northern Hikurangi (in the East around -38° to -40° latitude), with observed catalog being more productive. Also model catalog appears more productive in the Bay of Plenty (in the North around -38° latitude 176° longitude). From (*Shaw et al.*, 2021)

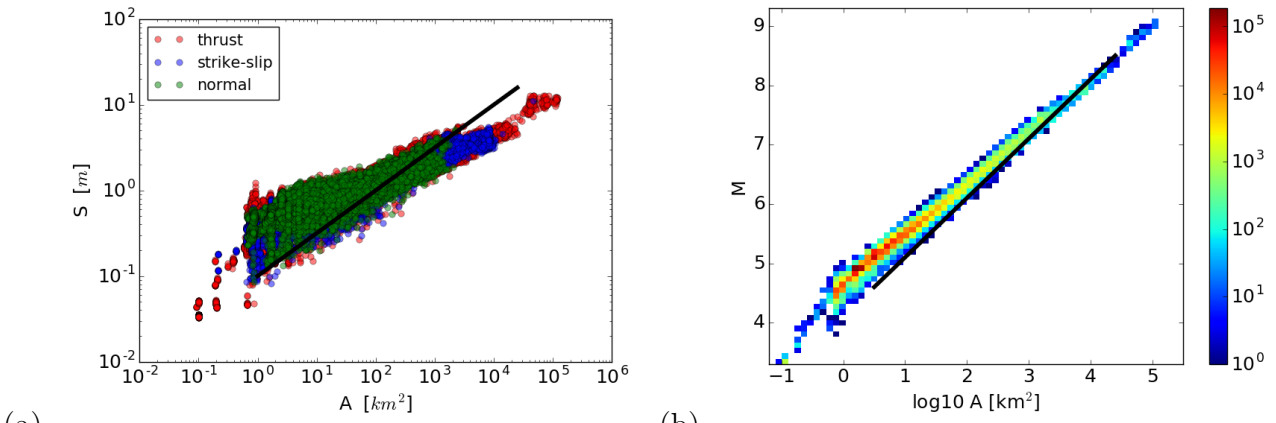

(a) (b)

Figure 6: Slip-size scaling plots of slip versus area and magnitude versus area are shown. (a) Scaling of slip S with Area A. Approximate scaling of slip versus the square root of area is seen, shown with solid black line. At the very small magnitudes there is some saturation in slip due to finite numerical resolution. Different mechanism events are shown with different colors. At high length/width aspect ratios, there is also saturation of slip with area due to finite seismogenic width, seen at the large strike-slip events in blue. Color coding is by mechanism of hypocenter. The few very large scattered occasional blue points ($A > 10^4 km$) on top of the red thrust subduction events indicate events which initiated on strike-slip faults but then propagated on continuing as large subduction events. (b) Magnitude-area scaling, histogram density plot. Units are number of counts per histogram bin. Color on log scale. Solid black line shows linear scaling of magnitude with log_{10} area scaling, for reference. Saturation of slip due to discretization effects at low magnitudes, leading to deviations above the line at small magnitudes, are not expected to impact hazard estimates. From (*Shaw et al.*, 2021)

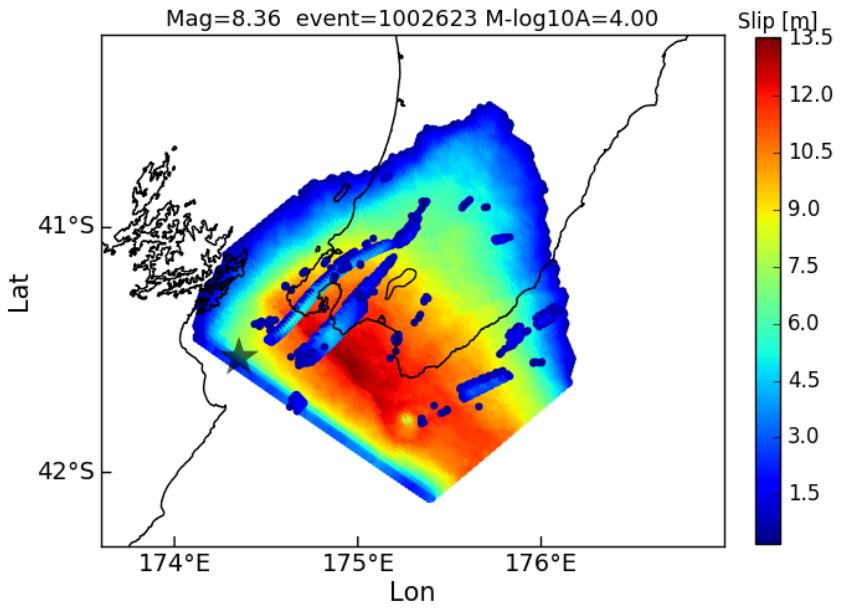

Figure 7: Map view of large **M**8.4 subduction event which also ruptures coseismically a number of upper plate faults. Main subduction fault is the Southern Hikurangi. The next largest participating faults by area are the Wellington, Wairarapa, and BooBoo faults, respectively. Color indicates slip in meters. The event initiates on the subduction interface at the epicenter indicated by the grey star. In this event the difference between the measured magnitude and measured source area is $\mathbf{M}-log_{10}A = 4.0$, which is consistent with values from average subduction scaling relations. From (*Shaw et al.*, 2021)

Preprint using simulator to improve estimates of multifault ruptures

" Enumerating Plausible Multifault Ruptures in Complex Fault Systems with Physical Constraints", (*Milner, Shaw, and Field, 2021*)

We propose a new model for determining the set of plausible multifault ruptures in an interconnected fault system. We improve upon the rules used in the Third Uniform California Earthquake Rupture Forecast (UCERF3) to increase connectivity and the physical consistency of ruptures. We replace UCERF3's simple azimuth change rules with new Coulomb favorability metrics and increase the maximum jump distance to 15 km. Although the UCERF3 rules were appropriate for faults with similar rakes, the Coulomb calculations used here inherently encode preferred orientations between faults with different rakes. Our new rules are designed to be insensitive to discretization details and are generally more permissive than their UCERF3 counterparts; they allow more than twice the connectivity compared to UCERF3, yet heavily penalize long ruptures that take multiple improbable jumps. The set of all possible multifault ruptures in the California fault system is near-infinite, but our model produces a tractable set of 298,542 ruptures (a modest 18We describe the rupture building algorithm and its components in detail, and provide comparisons with ruptures generated by a physics-based multicycle earthquake simulator. We find that nearly twice as many ruptures generated by the simulator violate the UCERF3 rules than violate our proposed model.

In developing a new set of criteria to improve the rupture set feeding into rupture forecast inversions, we used a dialog with the simulator output to test the new Coulomb-based measures. Three figures below illustrate this dialog. Figure 8 illustrates the Coulomb interactions between faults used as a physical basis for building plausible ruptures. Care was taken to develop a series of measures based on coulomb interactions which were robust and insensitive to discretizations. Figure 9 shows a comparison of distributions of rupture jump azimuths using the previous UCERF3 filter, the emergent RSQSim simulated ruptures, and the new UCERF4 filters. We see a much better agreement of the new filters with the simulated ruptures. Figure 10 shows a comparison of the rate of simulated ruptures failing the previous UCERF3 rupture filters as compared with the new UCERF4 filters. We see also most of the ruptures which do fail are based on one or two subsections on large ruptures failing, which also supports the new approach as these indicate ruptures attempting to take branches and then dying out. Again we see better agreement of the new UCERF4 filters with the simulated ruptures as compared with the old UCERF3 filters.

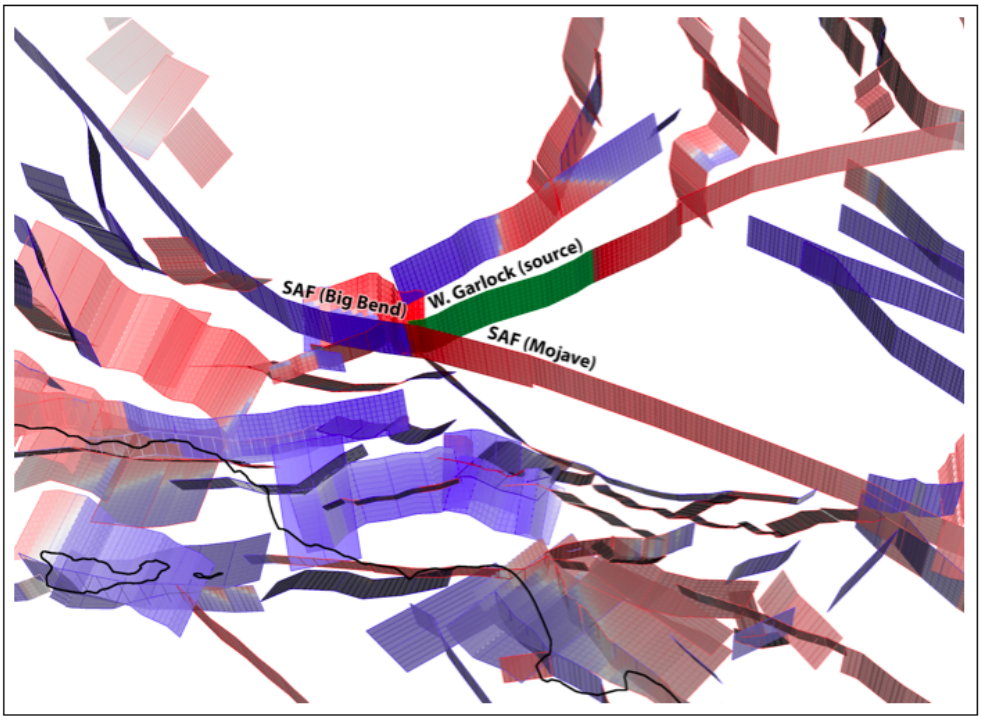

Figure 8: Figure illustrating Coulomb interactions incorporated into measures used to select multifault ruptures. 3D view looking north of faults from the Third Uniform California Earthquake Rupture Forecast (UCERF3) model broken up into 2 km x 2 km patches for Coulomb calculations. Patches overlap slightly in order to fill the fault surfaces completely. In this example, eight subsections of the Garlock fault are used as sources (green) and Coulomb stress changes are computed to all other patches (with contributions summed across all source patches). Receiver patches are colored by their sign with darker colors indicating greater amplitude, and subsection outlines are colored by the sum across all receiver patches (red is positive, blue negative). This shows the Coulomb-preferred corupture direction of the left-lateral Garlock Fault connecting to the Mojave section of the right-lateral San Andreas Fault (SAF). Coastlines are overlaid in black. From (*Milner, Shaw, and Field, 2021*)

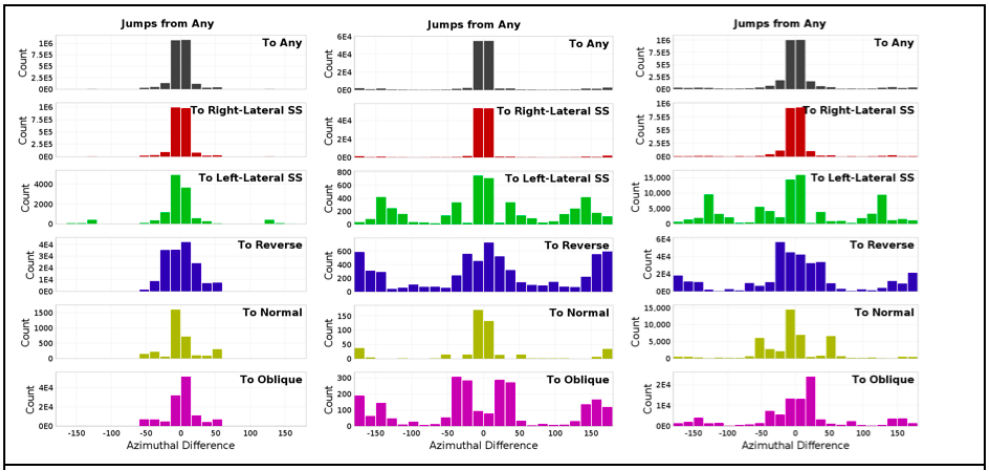

Figure 9: Comparison of distributions of jump azimuths in previous UCERF3 filter, RSQSim simulated ruptures, and new UCERF4 filter. The new filters show improved match with simulated ruptures. Jump azimuth changes allowed in (a) the UCERF3 model, (b) the comparison Rate-State Earthquake Simulator (RSQSim) model, and (c) the new model proposed here. Each differently-colored subplot (arranged in rows) corresponds to jumps from any type of fault to a fault of that type, e.g., the 3rd row from the top represents all azimuth changes at jumps either to, from, or between left-lateral strike-slip faults. From (*Milner, Shaw, and Field, 2021*)

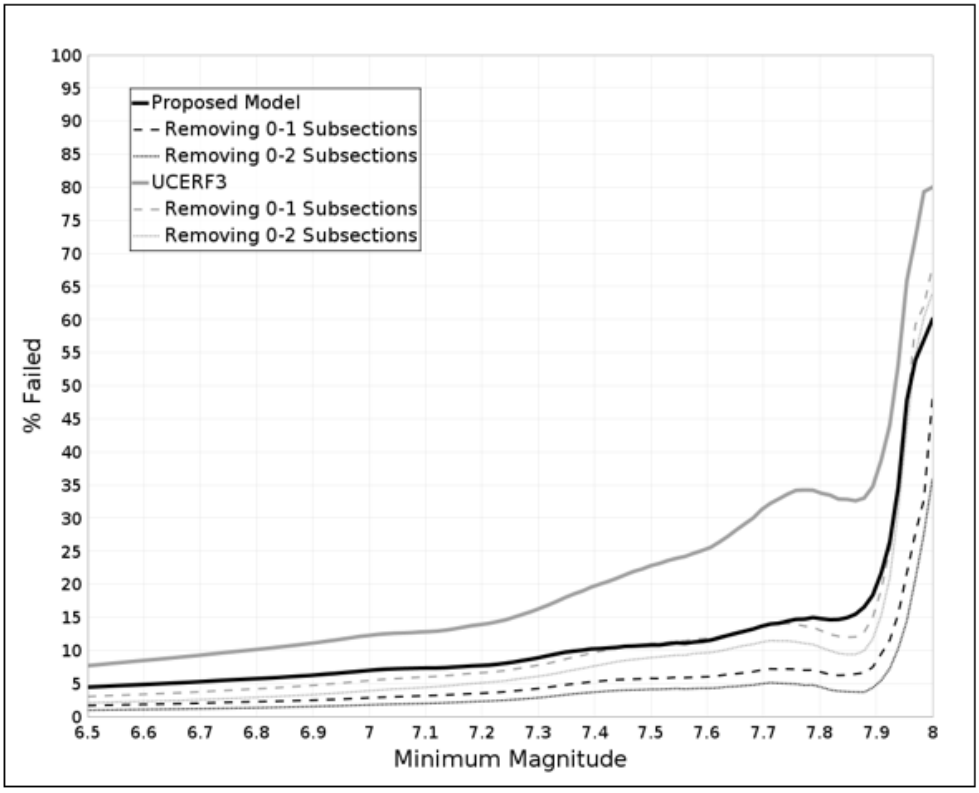

Figure 10: Comparison of fraction of RSQSim simulated ruptures failing UCERF3 filters compared with new UCERF4 filters. An improved match is seen with new filters. The rate at which ruptures from the RSQSim comparison model fail the plausibility filters used in UCERF3 (solid gray line) and proposed here (solid black line), as a function of magnitude. This excludes the minimum number of subsections per cluster filter, which is common to both models and was not intended to gauge rupture plausibility. Failure rates are also given for rupture subsets where up to one (dashed lines) and two (dotted lines) subsections are removed from an end of a participating fault section; this shows that the majority of failing ruptures are largely compatible except for one or two incompatible subsections. From (*Milner, Shaw, and Field, 2021*)

Acknowledgements

This material is based upon work supported by the U.S. Geological Survey under Grant No. G20AP00101.

Disclaimer

The views and conclusions contained in this document are those of the authors and should not be interpreted as representing the opinions or policies of the U.S. Geological Survey. Mention of trade names or commercial products does not constitute their endorsement by the U.S. Geological Survey.

References

Milner, K. R., B. E. Shaw, and E. H. Field, Enumerating plausible multifault ruptures in complex fault systems with physical constraints, *preprint*, 2021b.

Milner, K. R., B. E. Shaw, C. A. Goulet, K. B. Richards-Dinger, S. Callaghan, T. H. Jordan, J. H. Dieterich, and E. H. Field, Toward Physics-Based Nonergodic PSHA: A Prototype Fully-Deterministic Seismic Hazard Model For Southern California, *Bull. Seismol. Soc. Am.*, doi:10.1785/0120200216, 2021.

Shaw, B. E., Constant stress drop from small to great earthquakes in magnitude-area scaling, *Bull. Seismol. Soc. Am.*, *99*, 871, doi:10.1785/0120080006, 2009.

Shaw, B. E., K. R. Milner, E. H. Field, K. Richards-Dinger, J. J. Gilchrist, J. H. Dieterich, and T. H. Jordan, A physics-based earthquake simulator replicates seismic hazard statistics across California, *Science Advances*, *4*, eaau0688, doi:10.1126/sciadv.aau0688, 2018.

Shaw, B. E., B. Fry, A. Nicol, A. Howell, and M. Gerstenberger, An earthquake simulator for New Zealand, *preprint*, 2021.